Journal of Applied Sciences 4 (1): 110-117, 2004
ISSN 1607-8926

Numerical Simulation of Thermo-Chemical Non-Equilibrium Hypervelocity Flows

H. Ahmadikia and [1]E. Shirani
Assistant Professor of Engineering Department, Bu-Ali University, Hamadan, Iran
[1]Mechanical Engineering Department, Isfahan University of Technology, Isfahan, Iran

Abstract: Thermo-chemical non-equilibrium hypersonic 2-D and axisymmetric flows were numerically simulated by using Roe-Reimann flux splitting method. The fluid is air and it is modeled using five species and a chemical scheme with 17 reactions. In this work, viscous hypersonic flows over several objectives at high altitudes were simulated by considering chemically dissociated gaseous. The flow structures and aerodynamic forces and heat transfer were calculated and compared with the case were the fluid is perfect gas. The results show that the dissociation of gas affects very much the location of shock waves, amount of wall temperature and heat transfer. But it has little effect on the pressure. For the projectile, the results show that the dissociation reduces the wall temperature by 25%. This is an important factor in the design of a projectile. For hypersonic flow over a hemisphere body, excellent agreement is obtained between calculated values for the properties at the wall and those determined from experiments.

Key words: Dissociation, non-equilibrium, hypersonic flows, axisymmetric flows, hemisphere body, double ellipse body, Roe method

INTRODUCTION

For reentry flows at sufficiently high altitude and Mach number, the air in the region behind the bow shock is in chemically non-equilibrium state. Even for laminar flows, the problem is very complicated due to the large number of variables and partial differential equations required to describe the chemical and thermo-chemical quantities.

Non-dimensional Damokohler number is defined as $D_a=\tau_{trans}/\tau_{chem}$, where τ_{trans} is the characteristic time of translation and τ_{chem} is the characteristic time of chemical relaxation. Two limiting cases are $D_a<<1$, where the flow can be considered frozen and $D_a>>1$, where the flow is considered to be in the chemical equilibrium state. For Damokohler number between the two limiting cases, the flow is in non-equilibrium state. The mathematical model for flows with finite rate chemistry (non-equilibrium) is provided by the conservation laws of mass, momentum and energy, plus a set of equations for the non-equilibrium processes. The numerical simulation of such flows is time consuming and complicated due to the existence of different chemical species and wide range of the time scales.

Most of the steady-state solutions of hypersonic flows are computed by marching the unsteady governing equations, using explicit or implicit integration techniques. The explicit approach was very popular in mid 1980s due to its moderate demand on computer resource[1-3]. For faster reaction problems, the stiffness of the source terms may limit the permissible time step to very small values, resulting large computational times. Bussing and Murman[4] improved this numerical stability limitation by treating the chemical source terms in implicit manner and the convective terms in an explicit manner. Palmer and Venkatapathy[5] showed that with full implicit manner, the effective CFL number is high at Mach number over 30. The explicit algorithms experience convergence difficulties for Mach number over 30.

The development of algorithms for the Navier-Stokes equations with thermo-chemical non-equilibrium effects has been spurred to large extent by the desire to build the National Aero-Space Plane (NASP) in USA and other hypersonic vehicles. Calender[6,7], Liu and Vinokur[3], Grossman and Cinnella[8] and Wada *et al.*[9] are among those authors who have dealt with both thermal and chemically non-equilibrium flows and several investigators have developed computer codes with the capability for simulating portions of wide range of flight conditions[10,11]. Walter *et al.*[12] employed implicit methods to solve non-equilibrium flows with species transport and vibration energy equations are assembled over the domain or part of it and solved simultaneously in a coupled fashion. However, for typical hypersonic reacting problems, such a formulation results in a large system of equations that is quite demanding in terms of memory. Ait

Corresponding Author: E. Shirani, Mechanical Engineering Department, Isfahan University of Technology, Isfahan, Iran

Ali Yahi and Habashi[13] employed implicit Galerkin-finite elements method to solve non-equilibrium flows with gas dynamic, chemical species transport and vibration energy equations. Peigin *et al.*[14] employed thin layer Navier-Stokes equations for solving flow field over three-dimensional ellipsoid with species vibration energy equations. Solution of species vibration energy equations, results the increase of CPU time but it does not increase the accuracy of the problem.

In order to solve flow problems in hypersonic flights, one needs to develop an efficient code in the computational fluid dynamics. In this paper, the ability of a computer code developed by using Roe scheme applied to very stiff flow conditions, a high velocity at an altitude of over 70 km is examined. At the high temperature and Mach number flows, the number of equations for conservation of species could be very high. In this work, we have neglected ionization phenomena and the dissociation of air are assumed to have five neutral species; O, N, NO, O_2 and N_2.

MATERIALS AND METHODS

Governing equations: The compressible Navier-Stokes equations for 2-D and axisymmetric flows with non-equilibrium chemistry in the vector conservation form are as follows:

$$\frac{\partial \vec{Q}}{\partial t}+\frac{\partial \vec{E}_i}{\partial x}+\frac{\partial \vec{F}_i}{\partial y}=\frac{\partial \vec{E}_v}{\partial x}+\frac{\partial \vec{F}_v}{\partial y}+\vec{H} \qquad (1)$$

where, Q is the conserved variables, H is production rates and the inviscid fluxes are:

$$Q=y^m[\rho, \rho u, \rho v, \rho e_t, \rho_i]^T, \quad I=1, N-1 \qquad (2)$$

$$\vec{H}_i=[0, 0, m(p-\tau_{00}), 0, y^m \dot{\omega}_i]^T \qquad (3)$$

$$\vec{E}_i=y^m[\rho u, \rho u^2+p, \rho uv, (e_t+p)u, \rho u Y_i]^T \qquad (4)$$

$$\vec{F}_i=y^m[\rho vu, \rho uv, \rho v^2+p, (e_t+p)v, \rho v Y_i]^T \qquad (5)$$

where, u and v are Cartesian velocity components, e_t is total energy per unit volume, ρ is fluid density and p is static pressure and is given by the state equation. m=0 is for 2-D and m=1 for axisymmetric flows. The viscous flux vectors $\vec{E}_v$ and $\vec{F}_v$ and the shear stresses tensor for the full Navier-Stokes equations, along with more details on the modeling of the viscous terms for non-equilibrium gas are given by Walters *et al.*[12].

Eight conservation equations including two equations for momentum, one for total energy and five for species are used.

Chemistry model: The air is considered to be a mixture of five species (N_2, O_2, NO, N and O), each species is assumed to behave as a perfect gas. The temperature and pressure are calculated iteratively form the following equations:

$$p=\Sigma p_i=\Sigma \rho_i R_i T \qquad (6)$$

$$e_t=\rho h-p+\frac{1}{2}\rho(u^2+v^2) \qquad (7)$$

$$h_i=h_{fi}^{\circ}+\int_{Ref}^{T} C_{pi}dT, \qquad h=\sum h_i Y_i \qquad (8)$$

where, h°_{fi} and R_i are the heat of formation and gas constant of the i^{th} specie, respectively. $Y_i=\rho_i/\rho$ and c_{pi} are mass fraction and the specific heat at constant pressure of the i^{th} specie, respectively. Expressions for the specific heats as functions of temperature are obtained by using data from JANAF tables[15] and the curve fiting of the data by the following polynomial functions.

$$C_p/R=a_1+a_2T+a_3T^2+a_4T^3+a_5T^4+a_6T^5+a_7T^6+a_8T^7 \qquad (9)$$

where, a_1, a_2,... a_8 are constant. This relation is suitable for 100 to 20000 K.

In general for a mixture of N species, there will be the following J reactions:

$$v'_{1,j}X_1+v'_{2,j}X_2+\ldots.+v'_{N,j}X_N \underset{k_b}{\overset{k_f}{\leftrightarrow}} v'_{1,j}X_1+v''_{2,j}X_2+\ldots.v''_{N,j}X_N \qquad j=1,2,\ldots,J \qquad (10)$$

where, the $v'_{i,j}$ and $v''_{i,j}$ are the stoichiometric coefficients of the i^{th} specie in the j^{th} reaction. k_f and k_b are the forward and backward reaction rate constants, respectively. In the present study, a chemical reaction scheme consisting of 17 reactions was employed[16]. The forward and backward rates are determined by Arrehnious relations[17].

$$k_f=A_j T^{n_j}\exp(-E_j/T), \quad k_b=A'_j T^{n'_j}\exp(-E'_j/T) \qquad (11)$$

The coefficents A_j, E_j and n_j are given by Kang *et al.*[18].

For non-equilibrium chemistry, the rate of production of the i^{th} specie may be written as:

$$\dot{\omega}_i=\frac{d\rho}{dt}=M_i(v''_{i,j}-v'_{i,j})\left[k_{f,j}\prod_{l=0}^{N}\left(\frac{\rho Y_l}{M_l}\right)^{v'_{l,j}}-k_{b,j}\prod_{l=0}^{N}\left(\frac{\rho Y_l}{M_l}\right)^{v'_{l,j}}\right], \quad i=1,2,\ldots,N \qquad (12)$$

where, M_l is the molecular weight of species l.

It is common to assume that Fick's law is valid for high temperature air mixture, with only binary diffusion being considered. If all species have the same Lewis number, it can be shown that the mass fraction of the each species

is constant across the boundary layer. The diffusion "velocity components, $\tilde{u}_i$ and $\tilde{v}_i$ (for the viscous flux terms)" are calculated by Fick's law:

$$Y_i \tilde{u}_i = -D_{im} \frac{\partial Y_i}{\partial x} \quad (13)$$

$$D_{im} = (1 - X_i) / \sum_{i \neq j}^{N} \frac{X_i}{D_{ij}} \quad (14)$$

where, D_{im} is effective binary diffusivity of the species in the gas mixture and X_i is the mole fraction of the i^{th} specie. The binary mass diffusivities are calculated using Bird model[19]. The molecular viscosity and thermal conductivity of air (without reaction) are determined from Schilichting[20] and Gerolymos and Vallet[21], respectively. The molecular viscosity and thermal conductivity of the gas mixture are determined from Kuo[22].

Numerical scheme: Various numerical schemes have been used to solve the set of equations governing chemically reacting flows. When the flow involves high chemical reaction rates and heat release, the explicit schemes are generally very slow to converge. Most implicit schemes, on the other hands, require the inversion of banded block matrices and become exceedingly expensive specially when the chemical system involves a large number of species. In the present study, the time derivatives are approximated by the second order backward difference, which is implicit. The fluxes are approximated by flux-splitting Roe's method[23-25] and the diffusion fluxes are approximated by the second order central difference scheme. The semi-discrete form of the inviscid part of the equation 1 is given by:

$$(\hat{Q}_{i,j})_\tau + (\bar{E}_{i+1/2,j} - \bar{E}_{i-1/2,j}) + (\bar{F}_{i,j+1/2} - \bar{F}_{i,j-1/2}) = RHS \quad (15)$$

where over bars denote numerically approximated vectors. A pseudo finite volume framework for the volume $V_{i,j}$ is obtained by the similarity relation $\hat{Q}_{i,j} = Q_{i,j} V_{i,j}$.

Roe scheme may violate the entropy condition when eigenvalues at the Roe averaged state vanish. The absolute value of eigenvalues, λ, are modified when they are below some small values. To prevent entropy deflection around the sonic lines, Harten and Hyman[26] entropy conditions are used. The minimum of two-gradient and Van Leer[27] limiter are also employed to prevent numerical oscillations. Shirani and Ahmadikia[28] have carefully examined the properties of different limiters. In this work suitable limiter is used for each case.

Boundary conditions: At an inflow boundary, the flow parameters are assumed uniform and equal to the known free stream conditions. At solid boundaries, the velocity components and the normal pressure gradient are set to zero. The outflow boundary conditions are obtained by means of extrapolation using zero gradients of the flow properties. For the axisymmetric flow, all gradients are set to zero along the axis of symmetry. The adiabatic boundary condition is considered at the solid surfaces.

A noncatalytic wall boundary conditions for chemically reacting flows has been considered. At this boundary, no chemical reactions occur and hence there is no diffusion of any specie at the wall. The mass fraction of nitrogen and oxygen at the outflow boundary are set to be equal to their free stream value (Y_{N2}=0.769 and Y_{O2}=0.233).

Grid generation: Generation of the structured grid in the regions with complex curvilinear boundaries is important subject in computational aerodynamics. The accuracy and efficiency of a numerical solution depend considerably on the quality of the grid employed.

In this work, the algebraic method of Eiseman[29] were used to generate the grid. In this method in addition to the solid surface, two arbitrary internal surfaces have been chosen and the grid points have been carefully identified at each surface. Then by means of interpolation and use of a third order polynomial, other grid points were calculated. The proper choice of the internal surfaces and the grid points distribution, on these surfaces, are important items in obtaining suitable computational grid. The grid points are obtained so that the grids are fine near the wall and are nearly orthogonal.

RESULTS

Three basic 2-D and axisymmetric blunt-body configurations were chosen and the flow around them were simulated by the present analysis. Numerical results are presented for a) flow over a double ellipse, b) flow over hemisphere nose with a straight cylindrical after-body and c) axisymmetric flow over a projectile. The first group describes the application of the Navier-Stokes equations with non-equilibrium gas model and the ability of the Roe's method for very high speed and high temperature flows. The second group presents validation of perfect and dissociated gas solution with experimental

Table 1: Details of double-ellipse body grid

$\Delta y_{min}/d$	$\Delta S_{min}/d$	Cells	Grid
0.00014	0.00151	160×50	1
0.000087	0.00101	220×75	2
0.000056	0.00062	290×100	3

data for blunt body with constant and low temperature boundary condition. The third group deals with a practical aspects of the problem that is given by Pishevar and Ahmadikia[30-32], Ahmadikia and Pishevar[33].

Flow over a double ellipse: Numerical solutions of two-dimensional viscous flows over a double ellipse are obtained at a free Mach number of 25 and an angle of attack 30°. The standard atmosphere at 75 km (p_∞=2.52 Pa, T_∞=205.3 K) is assumed. The free stream conditions for this flow have been chosen so that strong non-equilibrium chemical effects take place with a high level of molecular dissociation. In this case, the limiter introduced by Van Leer[27] and the entropy condition introduced by Harten and Hyman[26] are employed. Boyd and Gocken[34] solved the flow over a 1-m radius sphere at 70 km altitude (similar to this example) with continuum and particle methods. At this condition, the Knudsen number, based on the free-stream mean free path and sphere radius is 8×10^{-4}. They showed the continuum calculation produces good results.

The configuration of double ellipse is defined as by Ait-Ali-Yahia and Habashi[13] and Hayes *et al.*[35]:

$$\begin{cases} \left(\frac{x}{6}\right)^2+\left(\frac{v}{1.5}\right)^2=1 & r>0 \\ \left(\frac{x}{3.5}\right)^2+\left(\frac{v}{2.5}\right)^2=1 & x<0, y>0 \\ y=2.5,\ y=-1.5 & x>0 \end{cases} \quad (16)$$

To ensure that the results were not affected by grid size, the grid study was done. Table 1 shows the grid used in this study. Fig. 1 shows a 220×75 computational grid. The initial grid was generated algebraically by third order polynomial interpolation function. Fig. 2 shows the computed surface temperature distributions on the double ellipse body using three types of the grid. The results show that 220×75 grid is fine enough and can be used for this case.

Figure 3 presents convergence history of the three grids for non-reacting flows. For 220×75 grid size, the residual of mass in the computational domain reduces to 10^{-14} after 3000 steps. Temperature contours for the dissociated gas through the flow region is shown in Fig. 4. The minimum and maximum values of mass fraction of O_2 are 0.01 and 0.233, respectively. The maximum mass fraction of O is 0.178. The contours of the mono-atomic oxygen concentration are shown in Fig. 5

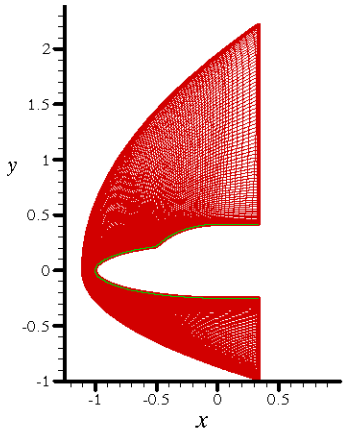

Fig. 1: Computational grid over a double ellipse

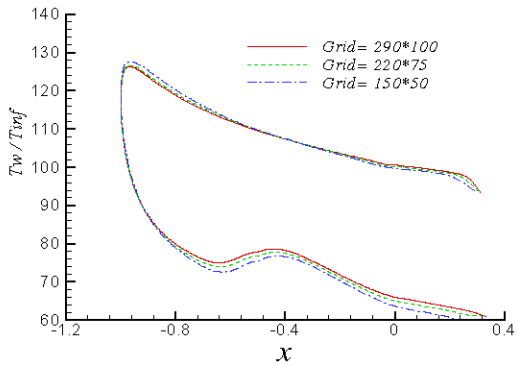

Fig. 2: Effects of different grid on computed surface temperature distribution

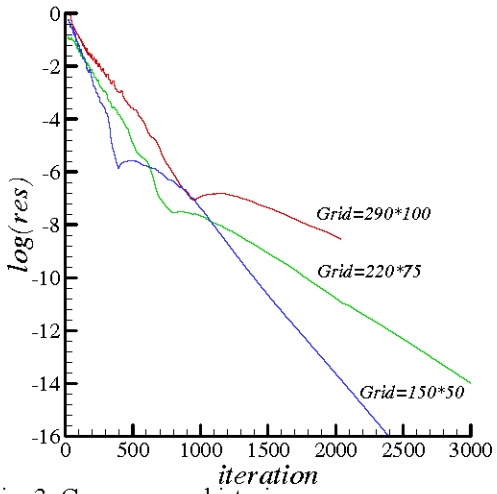

Fig. 3: Convergence histories

Flows over a hemisphere: The second test case consists of supersonic steady flow over a hemisphere nose with radius of 3.175cm and a straight cylindrical after-body. The free stream properties were described by standard atmospheric condition at an altitude of 30.48 km

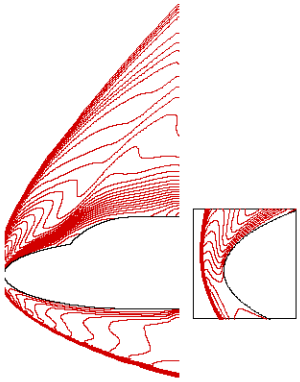

Fig. 4: Temperature counter on the double ellipse

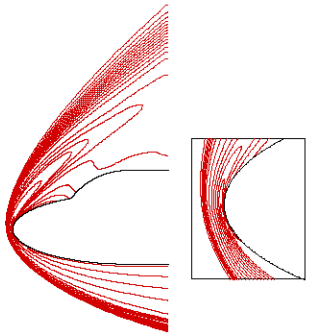

Fig. 5: Distribution of mass fraction of O, (y_{min}=3.3e^{-6}, y_{max}=0.233)

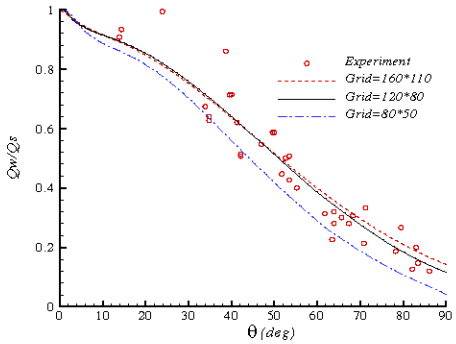

Fig. 6: Effect of different grid on surface heat transfer distribution

(T_∞=218 K and p_∞=1.081 Pa). The free stream Mach number and the characteristic Reynolds number are 12 and 1.36×10^5, respectively. The surface temperature is 555 K. This test case was proposed in the Workshop on Hypersonic Flows for Reentry Problems Abgrall *et al.*[36] and experimental results were obtained by Vetter *et al.*[37] for the same free stream conditions over a sphere. The free stream enthalpy for this case is much lower than that of the pervious case; hence the level of molecular dissociation in the flow region is expected to be much lower.

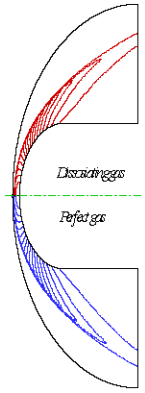

Fig. 7: Comparison of temperature contours over a hemisphere body for perfect and dissociated gas

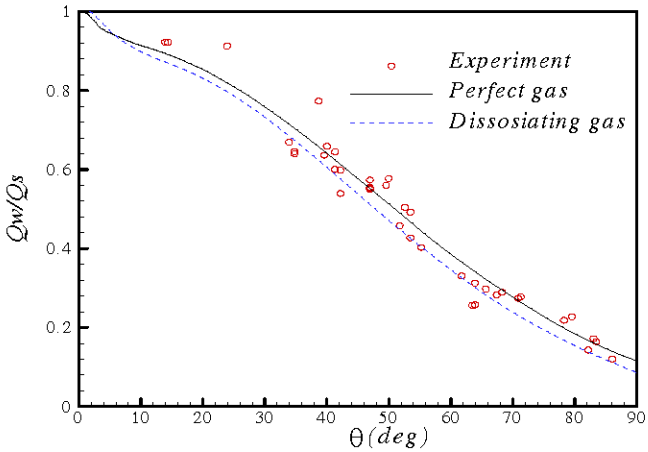

Fig. 8: Comparison of surface heat transfer distribution for a hemisphere body for perfect and non-equilibrium gas model

Three types of grids were considered for this case. The computed heat transfer distribution at the surface for three grid sizes and the experimental data given by Hayes *et al.*[35] are shown in Fig. 6. The results show that grid size, 180×120 is good.

Figure 7 shows comparison of temperature contours over a hemisphere body for perfect and dissociated gas. The range and increment of the contour levels are the same for all plots to facilitate comparison between the perfect and dissociated gas. The standoff distance differs between perfect and dissociated air mixture that is, the normal shock wave is closer to the stagnation point 19.5%, when compared with the perfect gas case. However, down stream from the stagnation point the shock-layer behavior are similar. The high density in the shock layer for the dissociated gas is a consequence lower temperature, resulting from a wider distribution of energy into additional internal degrees of freedom. The lower ratio of the specific heat of the dissociated air is

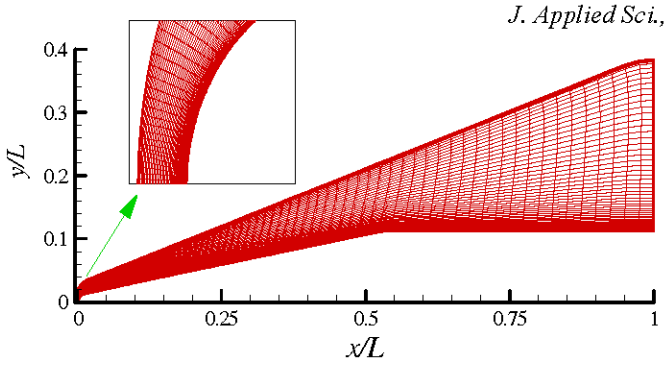

Fig. 9: Computational grid for projectile, altitude 70 km, Mach No. 18

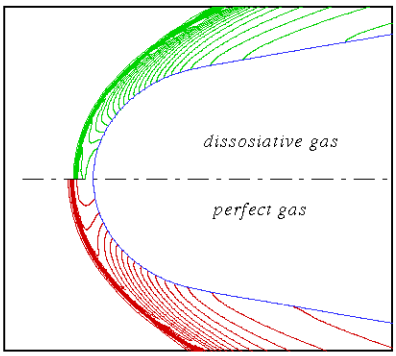

Fig. 10: Comparison of temperature contours for flow over a projectile

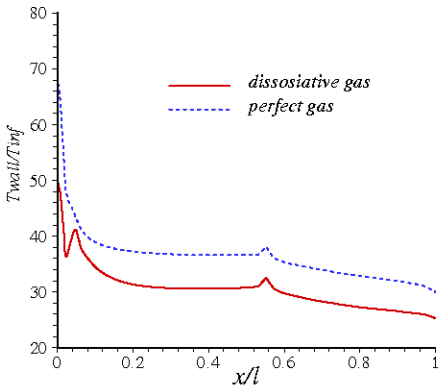

Fig. 11: Temperature distribution along the surface for perfect and dissociated gas

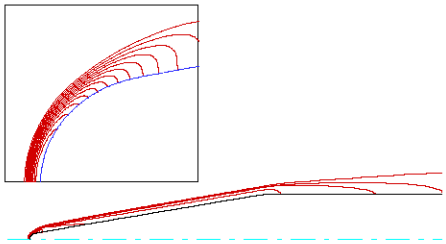

Fig. 12: Oxygen (O2) mass fraction contours for flow over a projectile

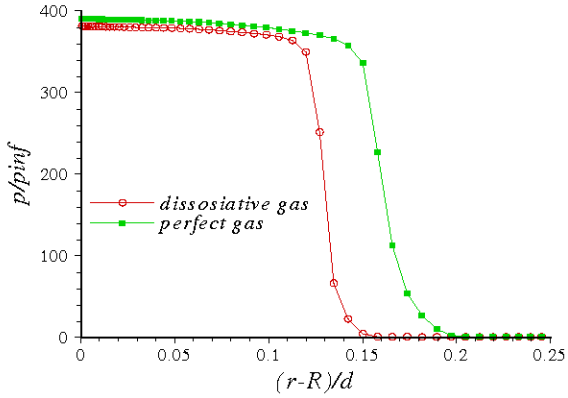

Fig. 13: Pressure distribution along the stagnation line for perfect and dissociated gas

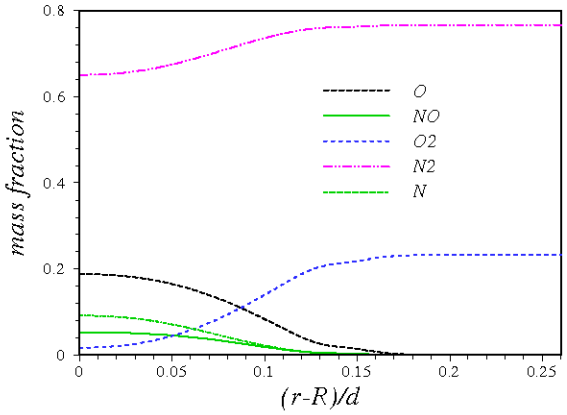

Fig. 14: Distribution of species mass fraction along the stagnation line

caused by a much rapidly expanded process in the shock layer. The bow shock wave attenuation into a Mach wave is accelerated by the dissociating phenomenon.

Comparison of wall heat transfer distribution for a hemisphere body for perfect and non-equilibrium gas model is shown in Fig. 8. The heat transfer to the wall is noticeable at the stagnation point and gradually diminishes away from this point. The calculated stagnation heat transfer at stagnation point for reacting flow compares well with that predicted experimentally. The effect of shock layer on the skin friction coefficient due to the dissociating phenomenon is considered. The maximum skin friction due to the dissociating phenomenon is 50% higher than its value for perfect gas case. However, the viscous force amounts to the less than 0.03% of the total drag force. The stagnation pressure in the dissociated case is 5.1% more than in perfect gas case and the maximum temperature in the shock layer is 6495K compared with 5043K for the perfect gas case. For this range of the temperature, the ionization is not taken place

and the five-component model used in this paper is reasonable.

Flows over a projectile: Numerical solutions of axisymmetric viscous flows over a projectile are considered. The free-stream Mach number is 18 and the altitude is 75 km (p_∞=2.52 Pa, T_∞=205.3 K). In this case, fluid is continuum and there is no ionization. Minimum of two-gradient limiter, Van Leer[27] and Harten and Hyman[26] entropy condition is employed. The flow over the projectile has been considered previously by Pishevar and Ahmadikia[30-32], Ahmadikia and Pishevar[33]. The grid study has been done and a suitable grid is shown in Fig. 9. The number of grid points are 120×55 and $\Delta s_{min}/d = 2.6\times10^{-4}$ and $\Delta y_{min}/d = 1.7\times10^{-7}$.

Figure 10 shows the temperature contours for perfect gas and dissociated gas cases. As shown in the Figure there is large difference between two cases, which is due to the dissociation of gas near the normal shock wave.

Only slight differences of the wall pressure are observed between the results obtained for perfect and dissociated gas, but large differences of the temperature are observed for perfect and dissociated gas cases. Since dissociation is endothermic, the temperature is reduced for the dissociated gas and the corresponding stagnation temperature for the reacting gas is about 40% less than for the perfect gas. The temperature distributions along the surface for the perfect and dissociated gas are shown in Fig. 11. The pick temperature in the shock layer is 67.4 T_{inf} for reacting flow and is 50.4 T_{inf} for perfect gas. Satofuka and Morinishi[38] used this property and by adding a specific material from aluminum chloride at the nose, due to the dissociation of the material, it observes energy and reduces the heat transfer at the wall.

The contours oxygen mass fraction for flow over a projectile is shown in Fig. 12. The O_2 dissociation occurs gradually over the whole shock layer, but only a small amount of N_2 dissociates near the body surface. O_2 dissociate completely in a thin layer behind the shock, whereas the N_2 dissociation occurs over the whole field, with steeper gradients behind the shock and the body surface.

Figure 13 shows pressure distribution along the stagnation line for perfect and dissociated gas. The Figure demonstrates the reduction of the stand off distance of the shock wave compared with the perfect gas. The decrease of the stand off distance of the bow shock wave leads to a corresponding thinner shock layer induced by the dissociated air. As is expected, the upwind TVD model sharply captures the shock waves in two or three computational cells.

Mass fraction of the five species, O_2, N_2, NO, N and O, along the stagnation line, are shown in Fig. 14. The temperature of the flow is not sufficiently high to noticeably produce the nitrogen atoms. The maximum mass fraction of N_2, O, NO and N are 0.767, 0.191, 0.0565 and 0.0993, respectively.

The non-equilibrium hypersonic flow past the hemispherical body was successfully simulated by solving the Navier-Stokes equations and using five species dissociated gas model and 17 reactions. The efficient computational solution of the problem requires the proper modeling of the phenomena. It is shown that the numerical solution of Navier-Stokes using Roe flux splitting and implicit methods is capable of simulating the thermochemical nonequilibrium steady flow over 2-D and axisymmetric blunt bodies at the high-speed flows. The Roes method with five species non-equilibrium gas flow provides an effective method for solution of hypersonic blunt bodies.

For the flow over a projectile with M_∞=18, the dissociation of the gas causes 25% reduction of temperature at the nose. This property drops the wall temperature and is used for selection of materials when the projectile is designed. Although the dissociation phenomena reduces the wall temperature considerably, it does not change the wall pressure and therefore the pressure drag remains unchanged.

REFERENCES

1. Eberhardt, S. and K. Brown, 1986. A shock capturing technique for hypersonic chemically relaxing flows. AIAA., pp: 86-0231.
2. Glaz, M.M., P. Collela, J.P. Collins and R.E. Ferguson, 1988. Non-equilibrium effects in oblique shock-wave reflections. AIAA. J., 26: 698-705.
3. Liu, Y. and M. Vinokur, 1989. Non-equilibrium flow computations. I. An analysis of numerical formulations of conservation laws. J. Computational Physics, 83: 373-397.
4. Bussing, T.R.A. and E.M. Murman, 1985. Finite volume method for the calculation of compressible chemically reacting flows. AIAA., pp: 85-0331.
5. Palmer, G. and Venkatapathy, 1995. Comparison of non-equilibrium solution algorithms applied to chemically stiff hypersonic flows. AIAA. J., 33: 1211-1219.
6. Calender, G., 1989. On the computation of shock shape in nonequilibrium hypersonic flows. AIAA. Nevada, USA., pp: 89-0312.
7. Calender, G., 1989. The Computation of weakly ionized hypersonic flow in thermo-chemical nonequilibrium. Ph.D. Thesis, Stanford University, USA.

8. Grossman, B. and P. Cinnella, 1990. Flux-split algorithms for flows with non-equilibrium chemistry and vibrational relaxation. J. Computational Physics, 88: 131-168.
9. Wada, Y., H. Kubota, S. Ogawa and T. Ishiguro, 1989. A generalized Roe's approximate Reimann solver for chemically reacting flows. AIAA. Nevada, USA., pp: 89-0202.
10. Palaniswamy, S., S.R. Chakravarthy and K. Ota, 1989. Finite rate chemistry for USA-series codes: formulation and applications. AIAA. Nevada, USA., pp: 89-0200.
11. Hoffman, J.J., 1989. Development of an algorithm for the th9ree-dimensional fully-coupled Navier Stokes equations with finite rate chemistry. AIAA. Nevada. USA., pp: 89-0670.
12. Walters, R.W., P. Cinnella, D.C. Slack and D. Halt, 1992. Characteristic-based algorithm for flows in thermo-chemical non-equilibrium. AIAA. J., 30: 1304-1313.
13. Ait-Ali-Yahia, D. and W.D. Habashi, 1997. Finite element adaptive method for hypersonic thermo-chemical non-equilibrium flows. AIAA J., 35: 1294-1302.
14. Peigin, S., V. Kazakov, M.M. Druguet, S. Seror and D.E. Zeitoun, 2001. Three-dimensional thermo-chemical non-equilibrium viscous flow over blunt bodies with catalytic surface. AIAA. J., 39: 626-636.
15. Stull, D.R. and H. Prophet, 1971. JANAF thermo-chemical tables. 2nd Ed., National standard reference data system NBS37, pp:1533-1667.
16. Park, C., 1985. On convergence of computation of chemically reacting flows. AIAA., pp: 85-0247.
17. Glassman, I., 1977. Combustion Academic press, NY.
18. Kang, S.W., W.L. Jones and M.G. Dunn, 1973. Theoretical and measurement electron-density distributions at high altitudes. AIAA. J., 11: 141-149.
19. Bird, R.B., 1962. Diffusion in multi-component gas mixtures. 25th Anniversary Congress Society of Chemical Engineering (Japan), 1961, Published in Abbreviated form in Kagaku, 26: 718-721.
20. Schilichting, H., 1979. Boundary-layer theory. McGraw-Hill, NY, pp: 327-339, 60-63.
21. Gerolymos, G.A. and I. Vallet, 1996. Implicit computation of three-dimensional compressible Navier-Stokes equations using k−ε closure. AIAA. J., 34: 1321-1330.
22. Kuo, K.K., 1986. Principles of combustion John Wiley and Sons, pp: 668-671.
23. Roe, P.L., 1981. The use of the Reimann problem in finite difference schemes. Lecture notes in physics, 141: 354-359.
24. Roe, P.L., 1985. Some contributions of modeling of discontinuous flows. Lecture notes in applied mathematics, pp: 163.
25. Roe, P.L., 1986. Characteristic-based schemes for the Euler equations. Annual review of fluid mechanics, 18: 337-365.
26. Harten, A. and J.M. Hyman, 1983. Self adjusting grid methods for one-dimensional hyperbolic conservation laws. J. Computational Physics, 50: 235-269.
27. Van Leer, B., 1986. Flux vector splitting for the Euler equations. Annual review of fluid mechanics, 18: 337-365.
28. Shirani, E. and H. Ahmadikia, 2001. Evaluation of Roe's method using different limiters to numerically simulate supersonic axisymmetric and two-dimensional viscous flows. Isteghlal J., IUT, Iran, pp: 111-124.
29. Eiseman, P.R., 1970. A multi-surface method of coordinate generation. J. Computational Physics, 33: 118-150.
30. Pishevar, A.R. and H. Ahmadikia, 2000. Numerical simulation of turbulence viscous flow on multi-stage missile. In proceedings of the 8th international ISME conference, Iran, pp: 893-901.
31. Pishevar, A.R. and H. Ahmadikia, 2001. On credibility of an algebraic turbulence model in predicting two-dimensional injection flows. Iranian J. Sci. Technol., Trans. B., 25: 231-240.
32. Pishevar, A.R. and H. Ahmadikia, 2002. Quasi-static viscous simulation of missile staging. Isteghlal J., IUT., 15: 141-150.
33. Ahmadikia, H. and A. Pishevar, 2000. Quasi-Static inviscid simulation of missile staging. In proceedings of the 6th fluid dynamics conference, Tehran, Iran, pp: 70-80.
34. Boyd, D.B. and T. Gocken, 1994. Computation of axisymmetric and ionized hypersonic flows using particle and continuum methods. AIAA J., 32: 1828-1835.
35. Hayes, W.D. and R.F. Probstein, 1959. Hypersonic flow theory. Academic, NY.
36. Abgrall, R., J.A. Desiideri, R. Glowkinski, M. Mallet and J. Periaux, 1991. Hypersonic flow for reentry problems. 3, Springer-Verlag, NY.
37. Vetter, M., H. Olivier and H. Gronig, 1991. Flow over double ellipsoid a sphere-experimental results, Hypersonic Flow for Reentry Problems. 3, Springer-Verlag, NY.
38. Satofuka, N. and K. Morinishi, 1994. Method of lines approach to computational fluid dynamics using rational Runge-Kutta time stepping scheme. Frontiers of computational fluid dynamics. John Wiley and Sons, pp: 189-213.